



Site Selective Detection of Methane Dissociation on Stepped Pt Surfaces

A. Gutiérrez-González¹ · M. E. Torio^{2,3} · H. F. Busnengo^{3,4} · R. D. Beck¹

© Springer Science+Business Media, LLC, part of Springer Nature 2019

Abstract

We report a combined experimental and theoretical study comparing methane dissociation on three different platinum surfaces Pt(111), Pt(211), and Pt(110)-(1 × 2). Reflection absorption infrared spectroscopy (RAIRS) was used to detect chemisorbed methyl species formed by dissociative chemisorption of CH₄ on specific surface sites and to measure surface-site-specific sticking coefficients of CH₄ on the terrace, step, and ridge sites as function of incident translational energy. Methane dissociation is observed to be direct on all sites and diffusion of the chemisorbed methyl species is absent for surface temperature below 150 K. The experimental data are compared with the results of density functional (DFT) calculations that give minimum energy barriers for CH₄ chemisorption that properly account for the experimental relative site-specific reactivities. Also in agreement with experiments, DFT results predict a negligible effect of co-adsorbed H and CH₃ species on the vibrational frequency of a methyl group chemisorbed on terrace and step sites of Pt(211). However, the origin of the red-shift of the RAIRS peak of CH₃ chemisorbed on terrace sites compared with that on step sites of Pt(211) remains elusive and still demands further investigation.

Keywords Pt surfaces · Methane · RAIRS · DFT

1 Introduction

The dissociative chemisorption of methane on a metal catalyst is known to be the rate-limiting step in the steam-reforming process, which is the principal industrial source of molecular hydrogen [1]. The hydrogen is needed for the synthesis of ammonia as well for combustion in fuel cells

among other applications. Due to its importance, the catalytic activation of methane has been extensively studied in surface-science [2–5].

A number of experimental and theoretical studies have explored the effect of translational and vibrational energy on the dissociation of methane for different catalytically active surfaces [6–14]. Quantum state resolved molecular beam studies proved methane chemisorption to be *mode-specific*, where the dissociation probability depends not simply on the reactant's total vibrational energy but differs for different isoenergetic vibrational modes by up to an order of magnitude [11]. Therefore statistical theories, assuming complete randomization of the initial vibrational energy prior to dissociation on the catalyst surface, do not provide an accurate description of the reaction dynamics for methane chemisorption [15–17]. In contrast, dynamical models including quasi-classical and quantum theories are needed to accurately describe the energy flow and activation of the methane molecule approaching the metal catalyst [18–22].

Significant effort has been put in the collaboration between theory and experiment with the goal to arrive at a predictive understanding of this reaction in order to find optimal catalytic conditions for the dissociation of methane

✉ H. F. Busnengo
busnengo@ifir-conicet.gov.ar

✉ R. D. Beck
rainer.beck@epfl.ch

¹ Laboratoire de Chimie Physique Moléculaire (LCPM), École Polytechnique Fédérale de Lausanne (EPFL), 1015 Lausanne, Switzerland

² Centro Internacional Franco Argentino de Ciencias de la Información y de Sistemas (CIFASIS), CONICET-UNR, Bv. 27 de Febrero 210 bis (2000), Rosario, Argentina

³ Facultad de Ciencias Exactas, Ingeniería y Agrimensura, Universidad Nacional de Rosario, Av. Pellegrini 250 (2000), Rosario, Argentina

⁴ Instituto de Física Rosario (IFIR), CONICET-UNR, Bv. 27 de Febrero 210 bis (2000), Rosario, Argentina

[23, 24]. However, most surface science studies performed so far on methane dissociation have used single crystals cut along high symmetry crystallographic directions, which are not fully representative of the surface of real catalysts. The structural difference between the atomically smooth single crystals often used in surface science experiments and real catalysts containing defects such as steps, kinks and vacancies is known as the “structure gap” [25–27].

One way to start closing this structure gap is to study the role of a specific defect by using single crystals cut in ways to expose a well-defined arrangement of “defect” sites such as steps and kinks. One of the first such studies concerning methane dissociation on a stepped surface was reported by Gee et al. [28] who probed methane dissociation on a Pt(533) surface which consists of a periodic array of (111) terrace and (100) step sites. By comparing the reactivity of CH₄ on the stepped Pt(533) with a flat Pt(111) they observed a higher dissociation probability on the stepped surface, which they attributed to the presence of the (100) steps. However, the product detection methods that they used (King and Wells method [29] and O₂ titration) were not surface-site-specific and only measured total reactivity averaged over all surface sites present on the sample. In order to extract the reactivity of the step sites, the authors had to assume equal reactivity for the terrace sites on Pt(533) and Pt(111) which is not necessarily correct [30].

Papp et al. [31] studied methane dissociation on the stepped surfaces Pt(355) and Pt(322) using X-ray photoelectron spectroscopy (XPS). Both surfaces consist of five atoms wide (111) terraces separated by (111) and (100) steps, respectively. Methane reactivity was measured by recording carbon XPS line profiles following methane dissociation on Pt(111), Pt(355) and Pt(322). The XPS signal was deconvoluted into a series of peaks to resolve the contribution from terrace and step sites as well as due to C–H fragments produced by the intense X-ray radiation. Comparison of the signal ratios for the CH₃ peaks assuming identical vibrational fine structure for the terraces of the three surfaces indicated a similar reactivity for the step and the terrace sites, in contradiction with the study of Gee et al. [28]. However, on the stepped surfaces, methyl was found to occupy mostly the steps of the surface with about only 10–20% of the methyl coverage on the terraces. Assuming a similar reactivity for the terraces of the stepped surface and the terraces of the flat Pt(111) surface, the authors concluded that the higher coverage on the steps sites was due to a rapid diffusion to the step sites of the methyl groups initially formed on terrace sites at a surface temperature of 120 K.

The discrepancies between these two studies and the lack of further studies concerning the role of “defect sites” on the dissociation of methane on metals motivated us to perform a systematic study of this reaction on differently coordinated surface sites. The EPFL group has recently demonstrated the

surface-site-specific detection of chemisorbed methyl species on the step and terrace sites of Pt(211) [32] by reflection absorption infrared spectroscopy (RAIRS). RAIRS detection was used to measure the reaction probabilities for CH₄ dissociation on the steps and terraces of Pt(211) and compared to theoretical predictions obtained by the Reaction Path Hamiltonian (RPH) method for methane chemisorption based on density functional theory (DFT) developed by the group of Bret Jackson [32–34]. Both experiment and theory showed that the reactive sticking coefficients are higher on the steps than on the terraces of Pt(211) due to a lower dissociation barrier by at least 30 kJ/mol for steps compared to terraces. The experiments also showed that the dissociation is direct on both steps and terraces of Pt(211) and that diffusion of the methyl species from the terraces to the steps does not occur at T_s = 120 K in agreement with a calculated diffusion barrier of 65 kJ/mol [32].

DFT calculations are an important complement to surface site resolved experiments, in particular when the dissociation reaction can take place on several different adsorption sites. DFT can help to determine the adsorption geometry of methyl groups on different adsorption sites, aid in the assignment of the observed vibrational frequencies, and estimate the effect of lateral interactions between methyl groups, and the presence of co-adsorbed H atoms. To date, DFT calculations have been extensively used to investigate the stability of CH₃ on different adsorption sites of low- and some high-Miller-indices surfaces of Pt [32, 35–42]. All these studies agree that CH₃ adsorbs preferentially on top of a single Pt atom (i.e. top site) and that for stepped surfaces, the adsorption is more stable on Pt step atoms than on the terraces [32, 40, 41]. This stronger interaction with lower-coordination Pt atoms also entails a lower activation energy for CH₄ dissociation on step-edge sites than on the terrace sites, in line with larger sticking coefficients on the steps observed in our experiments [32].

Predicting vibrational frequencies of chemisorbed species by DFT is more challenging than the calculation of adsorption energies but can be very useful in order to confirm the assignment of the RAIR spectra to different adsorption sites. For the CH₃(ads) on Pt(211), we assigned the peak at 2886 cm⁻¹ to the symmetric C–H stretch of CH₃(ads) on terrace sites. A second peak, shifted by 17 cm⁻¹ to higher frequency was assigned to CH₃(ads) on the step sites, based on the comparison with the RAIR spectrum for CH₃(ads) on Pt(111) as well as the observed CH₃(ads) uptake which is much faster on the step than on the terrace sites [32]. A simple argument based on the stronger binding of CH₃(ads) on the step sites, suggests the opposite, i.e. a red-shift for the step compared to the terrace site similar to what is observed for CO species adsorbed on the step and terrace sites of Pt(211) [43]. Thus, the observed red-shift of the peak of

$\text{CH}_3(\text{ads})$ on the terrace with respect to the step is somewhat surprising.

Interestingly, the frequency of the symmetric C–H stretch mode of CH_3 on Pt(111) in the fcc-hollow sites is predicted by DFT to be lower than on the top sites, despite the CH_3 -surface bond in the former site being weaker than in the latter. Michaelides and Hu [36] concluded that the softening of the C–H bonds for CH_3 located on a fcc-hollow site is due to their stronger interaction with surface Pt atoms. For $\text{CH}_3(\text{ads})$ in the fcc-hollow sites, the C–H bonds are closer to the Pt atoms than for CH_3 chemisorbed on the top sites. A similar argument might explain the red-shift of the frequency of the symmetric stretching mode of $\text{CH}_3(\text{ads})$ on a terrace site of Pt(211) with respect to $\text{CH}_3(\text{ads})$ on a step-edge site, since in the latter case the C–H bonds are expected to be at a larger distance from the Pt surface atoms [32].

In this work, we extend our experimental studies for methane dissociation on Pt(111) and Pt(211), to Pt(110)-(1 × 2) using the site-specific detection capabilities of RAIRS for chemisorbed $\text{CH}_3(\text{ads})$ species reported by us recently [32, 44]. RAIRS detection of $\text{CH}_3(\text{ads})$ allows for surface-site-specific reactivity measurements for methane dissociation on platinum surfaces. We also present DFT results of adsorption energies, vibrational frequencies, and minimum energy barriers (E_b) for CH_4 dissociation on the three surfaces. In particular, we consider the influence of the choice of the exchange–correlation (XC) functional, the inclusion of long-range van der Waals dispersion forces, and the role of lateral interactions between adsorbates on the vibrational frequency of CH_3 chemisorbed on various sites of the three surfaces mentioned above.

2 Methodology

2.1 Experiments

The molecular beam-surface science apparatus used here has been described in detail previously [45]. Briefly, the apparatus consists of a three-fold differentially pumped molecular beam source coupled to an ultra-high vacuum (UHV)

chamber where reaction products adsorbed on the sample surface can be detected either by RAIRS or Auger Electron Spectroscopy (AES). Absolute sticking coefficient averaged over all surface sites can be determined by the King and Wells beam reflectivity method [29].

A continuous molecular beam was formed by skimming a jet expansion produced from a gas mixture of 1–3 bar stagnation pressure through a stainless steel nozzle. The translational energy of the molecular beam was controlled by seeding methane on He and by heating the nozzle ($T_N = 300\text{--}850$ K). The speed distribution of CH_4 in the molecular beam was measured by a time-of-flight (TOF) method using a chopper wheel in combination with an on-axis quadrupole mass spectrometer [46].

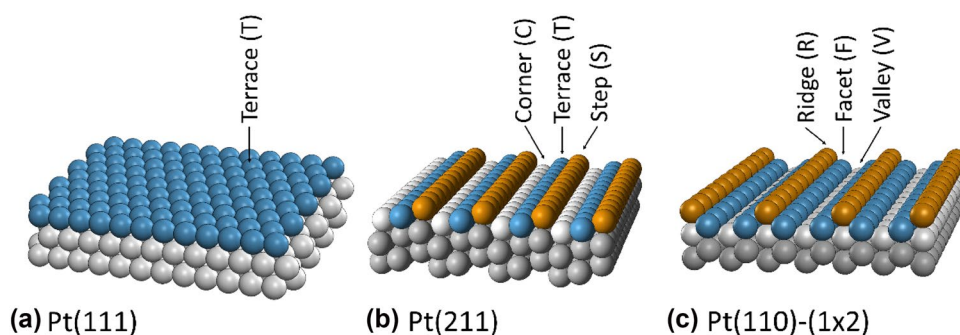
The molecular beam entered the UHV chamber with a base pressure of 5×10^{-11} mbar where it collided at normal incidence with the surface sample of 10 mm diameter. The three different single crystal surfaces used in the experiments shown in this study, Pt(111), Pt(211) and Pt(110)-(1 × 2), were obtained from Surface Preparation Labs and were cut within 0.1° of the specified crystal plane. The samples were mounted on a liquid nitrogen cryostat using 0.4 mm diameter tungsten wires. Surface temperature was controlled in the range of 90–1200 K using nitrogen cooling and by resistive heating of the tungsten wires.

Models of the surface structure for the three different Pt samples are shown in Fig. 1. The Pt(211) surface consists of three-atom-wide (111) terraces and one-atom-high (100) steps. Unlike the Pt(111) and Pt(211), the Pt(110) surface is reconstructed and exhibits a (1 × 2) missing-row reconstruction that leads to a corrugated structure consisting of alternating ridges and valleys [47].

Surface cleaning between measurements was done by exposing the surfaces to 5×10^{-8} mbar of O_2 at a surface temperature of 700 K for 5 min followed by annealing at $T_S = 1100$ K for 2 min. The surface cleanliness was confirmed using Auger Electron Spectroscopy (AES).

The methane dissociation products were detected by the RAIRS technique using an evacuated Fourier transform infrared (FTIR) spectrometer (Bruker Vertex V70) with an external InSb infrared detector.

Fig. 1 Models of the **a** Pt(111), **b** Pt(211), **c** Pt(110)-(1 × 2) surfaces with its different surface sites



The incident dose D of methane molecules on the surface can be calculated from [48]:

$$D = \frac{\Delta P S}{k_B T_g A} t \quad (1)$$

where ΔP is the methane partial pressure rise in the UHV chamber when the molecular beam is introduced into the UHV chamber, and it is obtained from a calibrated QMS. S is the effective pumping speed for methane in the UHV chamber, k_B is the Boltzmann's constant, T_g (K) is the gas temperature to the 298 K, A is the molecular beam spot area on the surface determined by AES and t is the deposition time. In order to express the dose in monolayers (ML), the surface atom density of the different surfaces has to be taken into account (1.5×10^{15} Pt atoms/cm² on Pt(111), 1.59×10^{15} Pt atoms/cm² on Pt(211) and 1.84×10^{15} Pt atoms/cm² on Pt(110)-(1 × 2)).

2.2 Theory

DFT calculations have been performed using a plane-wave basis set and the projected augmented wave method [49] to describe the interaction of valence electrons with atomic cores, as implemented in the VASP code [50–55]. The number of valence electrons considered for the atomic species H,

of exposed Pt atoms of the three surfaces under study here, we adopt and extend the nomenclature used in Ref. [32] for Pt(211). Thus, we qualify the exposed atoms of Pt(211) as: step (S), terrace (T), and corner (C). In Pt(111), there are only T atoms exposed. For Pt(110)-(1 × 2), the exposed atoms will be referred to as ridge (R), facet (F) and valley (V), respectively. In Fig. 1, S and R, T and F, and C and V atoms are represented as orange, blue, and gray spheres respectively. Figure 2, shows the optimum adsorption geometries we have obtained for CH₃ on T and S sites of Pt(211), on F and R sites of Pt(110)-(1 × 2) and on T sites of Pt(111).

In order to investigate possible effects of long-range van der Waals interactions on the frequencies of CH₃, we have also performed DFT calculations with the PBE-D3 method [57] and with the so-called optPBE-vdW XC functional [58].

We define adsorption energies of the single species X (X = CH₄, CH₃, H), as:

$$E_{ads}[X] = E[X/surface] - E[X] - E[surface] \quad (2)$$

where $E[X/surface]$, $E[X]$, and $E[surface]$ are the total energies of the full system X/surface, X in vacuum, and the clean surface respectively. Note that more negative values of $E_{ads}[X]$ correspond to more stable adsorption. For n CH₃ groups ($n = 1, 2$) co-adsorbed with m H atoms ($m = 0, 1, 2$), we also use $E_{ads}[CH_3]$ to denote the average adsorption energy, which we compute as follows:

$$E_{ads}[CH_3] = \{E[(nCH_3 + mH)/surface] - nE[CH_3] - mE[H] - E[surface] - mE_{ads}[H]\} / n \quad (3)$$

C and Pt were 1, 4, and 10 respectively. We used a smearing of width 0.1 eV, and an energy cut-off of 450 eV. Most of the calculations have been performed with the PBE semi-local XC functional [56]. The Pt(111), Pt(211), and Pt(110)-(1 × 2) surfaces have been modeled within the slab-supercell approach using $N = 5, 7$, and 7 Pt layers, and supercells 3×3 , 1×3 , and 1×3 respectively. The k-point meshes used to sample the first Brillouin zone were $5 \times 5 \times 1$ for Pt(111) and Pt(211), and $7 \times 7 \times 1$ for Pt(110)-(1 × 2). In all the geometry optimizations performed for adsorbate/surface systems, we kept the Pt atoms in the N_{bot} bottom layers fixed in their equilibrium positions obtained for the clean surface ($N_{bot} = 3$ for Pt(111), and $N_{bot} = 4$ for Pt(211) and Pt(110)-(1 × 2)), and we allowed full relaxation of the coordinates of all the other Pt atoms and those of the adsorbates. Geometry optimizations to look for local minima and saddle points in the adsorbate/surface interaction potential were performed using the quasi-Newton, conjugate-gradient, and dimer methods of the VASP code by setting IBRION = 1, 2, and 44 respectively (see [55] and references therein).

As mentioned above, it is well known that methyl groups chemisorb on the top sites of various low-Miller-index Pt surfaces, i.e. with the CH₃-surface bond directly involving a single Pt atom. For simplicity, to distinguish different types

The results presented here correspond to spin-restricted calculations except for the energies of CH₃ and H in vacuum. The vibrational frequencies are computed within the harmonic approximation as the square root of the eigenvalues of the Hessian matrix corresponding to the total energy of the system as a function of the atomic coordinates. To evaluate the Hessian matrix elements, we use the finite differences method with two displacements per atomic coordinate of CH₃ (one back and one forward) of 0.015 Å. A few test calculations considering 16 valence electrons for Pt atoms instead of 10 showed that the choice of the number of valence electrons of Pt barely affects the computed frequencies for CH₃(ads).

It might be argued that DFT plus the harmonic approximation might be not accurate enough to account for the measured 17 cm⁻¹ frequency shift between CH₃(ads) on Pt(211)-S and Pt(211)-T sites. However, even though DFT calculations tend to predict frequencies too large compared to experiment, the difference in vibrational frequency between different adsorption sites are much better reproduced. For instance, using the methodology described above, we were able to reproduce properly (both in absolute value and sign) the -17 cm⁻¹ shift between the RAIRS peaks corresponding to the stretching frequency of CO on Pt(211)-S and on Pt(211)-T [43].

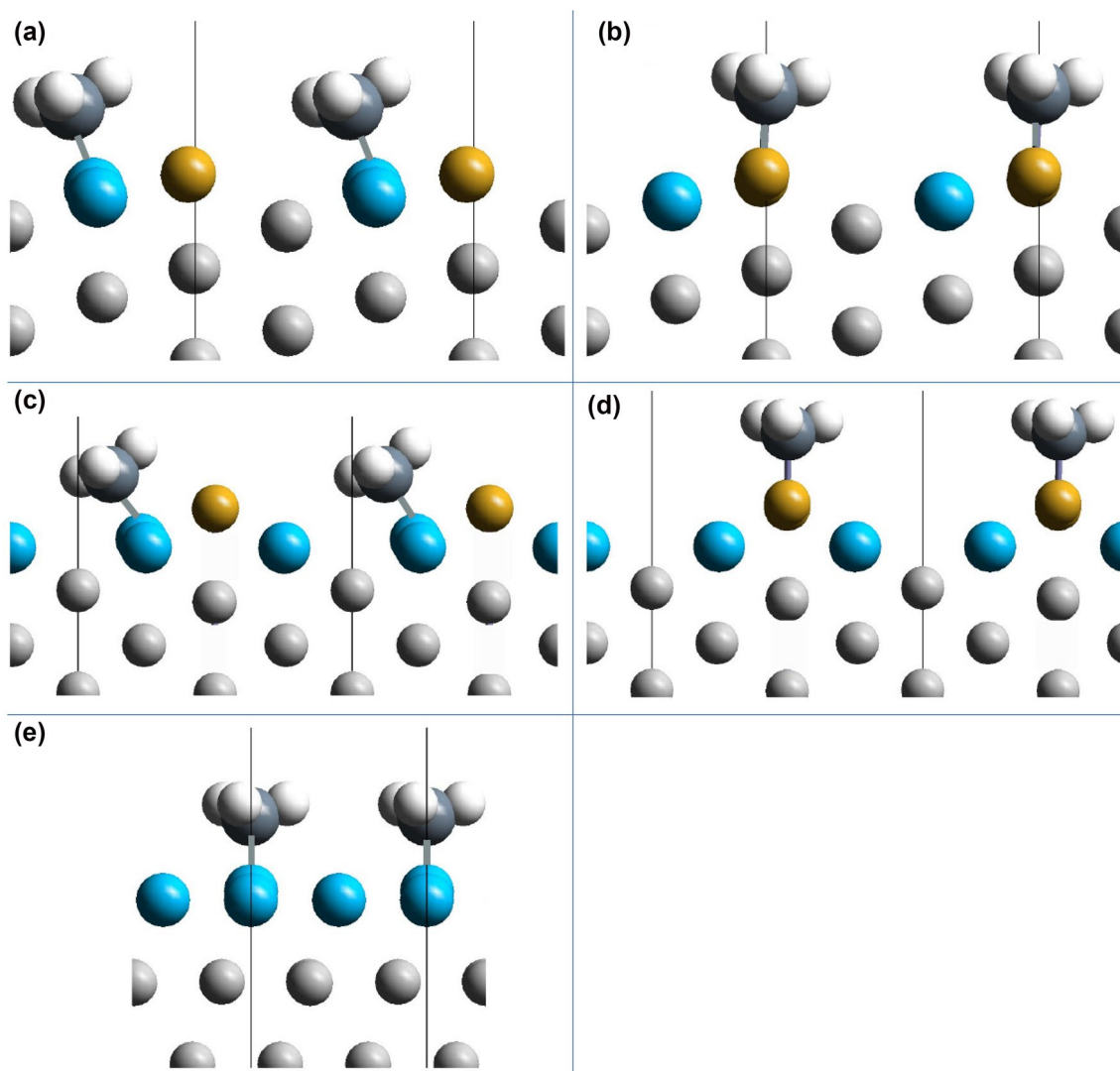


Fig. 2 Optimum DFT-PBE structure for CH_3 chemisorption on Pt(211)-T (a), Pt(211)-S (b), Pt(110)-(1 \times 2)-F (c), Pt(110)-(1 \times 2)-R (d), and Pt(111)-T (e). T, S, and C Pt atoms are represented in orange, blue, and gray respectively

3 Results and Discussion

3.1 Experiments

3.1.1 RAIR Spectra: Surface-Site-Selective Detection of Chemisorbed Methyl Groups

Figure 3 shows RAIR spectra following dissociative chemisorption of CH_4 on Pt(111), Pt(211), and Pt(110)-(1 \times 2). On Pt(111) at low surface temperature, CH_4 is known to dissociate directly on impact by cleaving a single C–H bond resulting in chemisorbed $\text{CH}_3(\text{ads})$ and $\text{H}(\text{ads})$ [45, 59, 60]. DFT calculations predict the dissociation to take place over the top site on Pt(111) with the $\text{CH}_3(\text{ads})$ product on the top site and $\text{H}(\text{ads})$ in a hollow site [61]. Temperature

program reaction measurements showed that $\text{CH}_3(\text{ads})$ is stable up to $T_s = 200$ K [62] on the terrace sites of Pt(111). For $T_s > 200$ K dehydrogenation leads to $\text{CH}(\text{ads})$ adsorbed on the hollow sites [62–64]. Figure 3a shows the RAIRS signal for the symmetric C–H stretch vibration of $\text{CH}_3(\text{ads})$ on Pt(111) with a single peak at 2881 cm^{-1} .

Recently, we have demonstrated the ability of RAIRS to distinguish between CH_3 adsorbed on the steps and terraces of Pt(211) [32]. Figure 3b shows a spectrum taken after dissociation of CH_4 on the Pt(211) with an incident translational energy of 65 kJ/mol. Comparison of the spectra taken following deposition under similar conditions on Pt(111) leads us to assign the RAIRS signals to $\text{CH}_3(\text{ads})$ on the step and terrace sites. The lack of a third peak, corresponding to $\text{CH}_3(\text{ads})$ on the corner sites, is consistent with a much

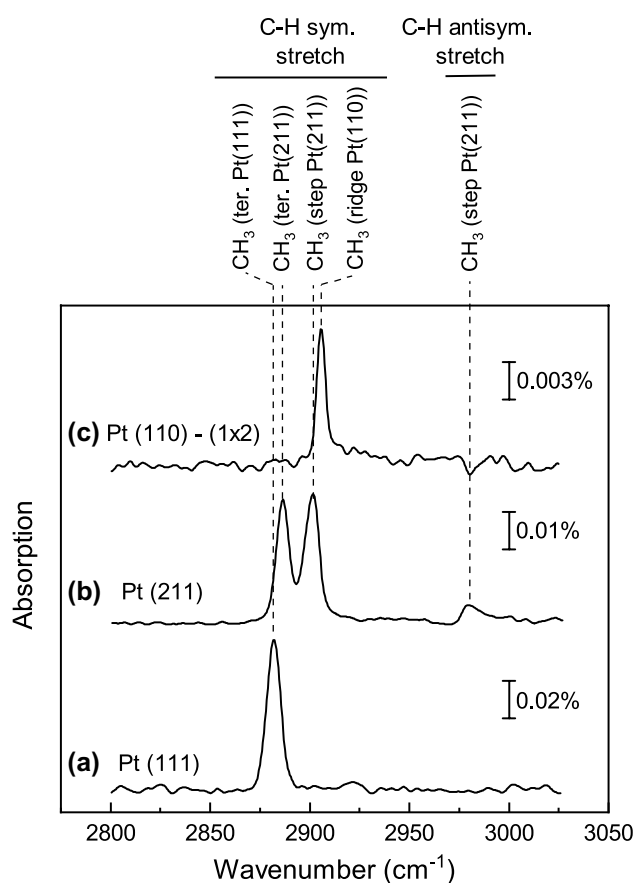


Fig. 3 RAIRS detection of $\text{CH}_3(\text{ads})$ adsorbed on a) Pt(111), b) Pt(211), and c) Pt(110)-(1 \times 2) at $T_S = 120$ K. $\text{CH}_3(\text{ads})$ was generated by dissociative chemisorption of CH_4 with incident kinetic energy in the range of 62–65 kJ/mol

higher barrier for dissociation on these sites, calculated by DFT as 183 kJ/mol [32].

A confirmation of the peak assignments for $\text{CH}_3(\text{ads})$ on the step and terrace sites was obtained by passivating the step atoms of the surface with $\text{CO}(\text{ads})$. CO adsorption on platinum surfaces has been extensively studied using RAIRS and its vibrational frequency on step and terrace sites are well-known [43, 65–67]. Following the saturation of the steps with $\text{CO}(\text{ads})$, we exposed the Pt(211) surface to a CH_4 molecular beam with 65 kJ/mol incident translational energy. Only the RAIRS signal at 2886 cm^{-1} was observed, confirming our assigned to $\text{CH}_3(\text{ads})$ on the terrace sites. Figure 4 shows a comparison of the spectrum obtained after deposition of CH_4 on the clean Pt(211) surface and the spectrum obtained at the same incident energy conditions on the Pt(211) where the steps were passivated by $\text{CO}(\text{ads})$. The observed vibrational frequencies are given with their assignments in Table 1.

In our most recent experiments, we extended the site-specific detection capabilities of RAIRS to the missing-row reconstructed Pt(110)-(1 \times 2) surface. Previously [68],

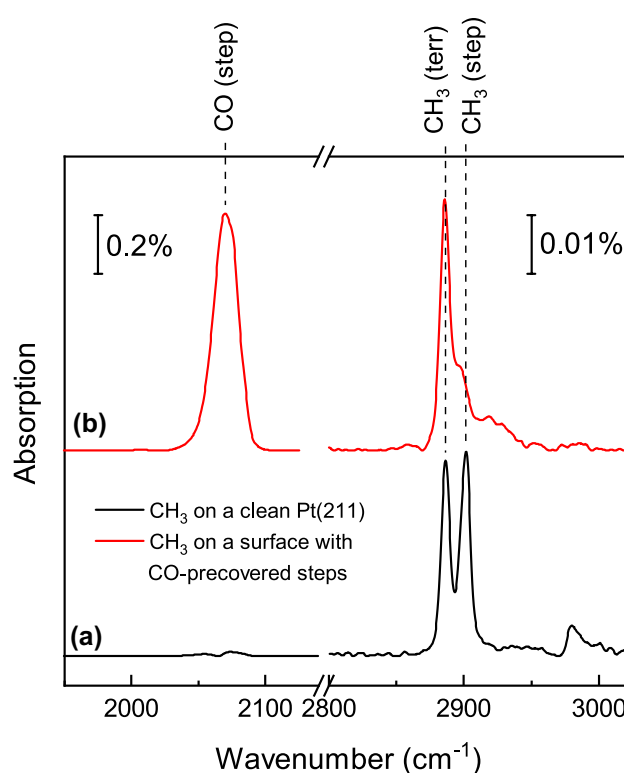


Fig. 4 RAIRS spectra following 45 min deposition of a 3% CH_4 in He molecular beam at $E_{\text{trans}} = 65$ kJ/mol at $T_S = 150$ K: a) on a clean Pt(211) surface, b) on a Pt(211) surface with steps passivated with $\text{CO}(\text{ads})$. Note the difference in absorption scales for $\text{CO}(\text{ads})$ and $\text{CH}_3(\text{ads})$ as indicated in the figure

Table 1 Assignments of RAIRS peaks observed for nascent methyl products of CH_4 dissociation on Pt(111), Pt(211) and Pt(110)-(1 \times 2) at $T_S = 150$ K

Surface	Site	Frequency (cm^{-1})	Mode assignment
Pt(111)	Terraces	2881	Symmetric C–H stretch
Pt(211)	Terraces	2886	Symmetric C–H stretch
	Steps	2903	Symmetric C–H stretch
		2979	Antisymmetric C–H stretch
Pt(110)-(1 \times 2)	Ridges	2905	Symmetric C–H stretch

Peak frequencies are taken from spectra in Fig. 3

we have measured the polar and azimuthal incident angle dependence for the dissociation probability of CH_4 on Pt(110)-(1 \times 2) by AES and K&W detection [68], which do not provide the site-selectivity of RAIRS. From the difference in the incident polar angle dependence of the sticking probability for incidence parallel and perpendicular to the missing rows, we concluded that the reactivity of CH_4 on the ridges should be much higher than in the valleys. Our experiments using RAIRS detection reported here confirm and strengthen this conclusion. Figure 3c shows a RAIR

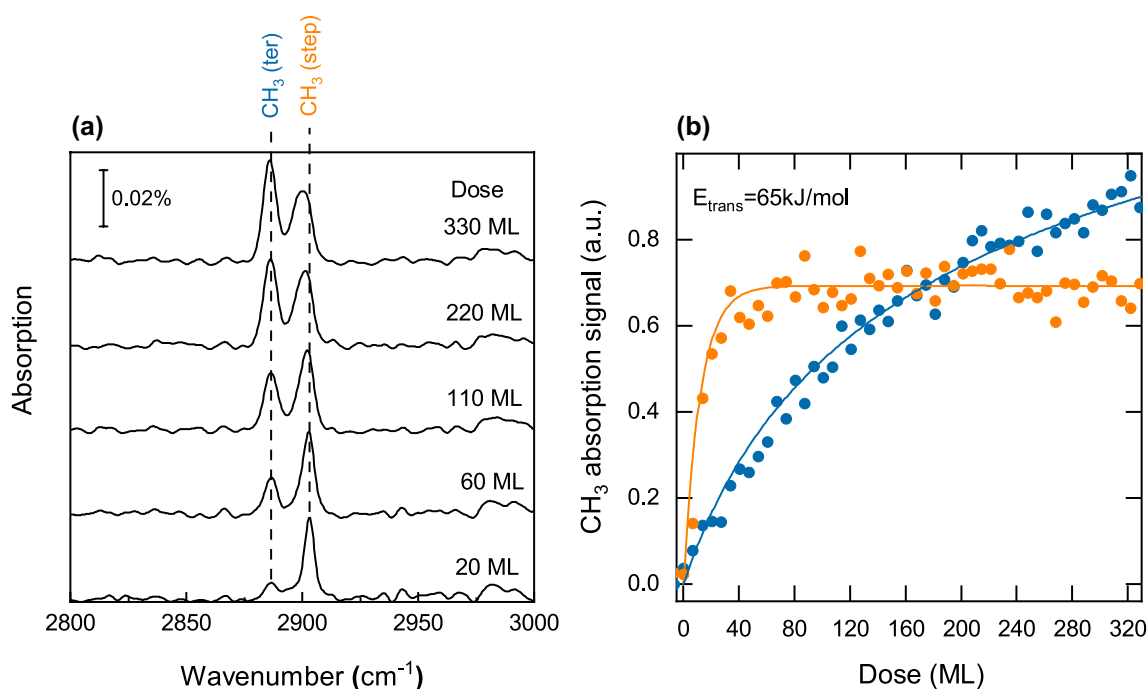


Fig. 5 **a** RAIR spectra taken during exposure of the Pt(211) surface at different incident doses of CH₄ at $E_{\text{trans}} = 65$ kJ/mol and $T_s = 120$ K. **b** Uptake curves for CH₃(ads) on the steps (orange) and on the terraces (blue) obtained integrating the area under the peaks for CH₃ adsorbed

spectrum measured following a 30 min deposition of CH₄ on the Pt(110)-(1 × 2) surface with an incident energy of 62 kJ/mol. We observe a single RAIRS peak in the C–H stretch region indicating that CH₃(ads) occupies only a single site on the Pt(110)-(1 × 2) surface. We assigned this peak at 2905 cm⁻¹ to the symmetric stretch vibration of CH₃(ads) on the ridge atoms of Pt(110)-(1 × 2) since we expect the ridge atoms to be the most reactive ones on this surface [68]. The assignment to CH₃(ads) on the ridge atoms of Pt(110)-(1 × 2) is consistent with the assignment of the 2903 cm⁻¹ peak to CH₃(ads) on the step atoms of Pt(211), since the two sites have the same coordination number of 7. Previous studies for CO adsorption have shown that the singleton frequency of CO(ads) on Pt is a linear function of the coordination number of the substrate atom where the CO molecule is adsorbed [69].

Since RAIRS does not interfere with the chemisorption process, it can be used to monitor uptake curves of the methane dissociation product CH₃(ads) during the molecular beam deposition. Figure 5a shows the evolution of the RAIR spectra with increasing incident dose for a 3% CH₄ in He molecular beam at 65 kJ/mol incident energy on the Pt(211) surface. Each spectrum is an average of 1024 scans with 4 cm⁻¹ resolution for an acquisition time of about 2.5 min. The absorption peak at 2903 cm⁻¹ assigned to CH₃(ads) on the step sites appears first, followed by the terrace peak at

on the step and terrace sites. The solid line corresponds to the fit to the experimental data points obtained using a Langmuir type uptake model [79]

2886 cm⁻¹. With increasing CH₃(ads) coverage, we observe a 2–3 cm⁻¹ red-shift of the step peak accompanied by some broadening while the frequency and linewidth of the terrace peak appears to be independent of coverage. The spectral changes observed for the step peak are likely due to a tilting of the methyl species on the steps when the terrace sites start to be populated by CH₃(ads).

Figure 5b shows the integrated peak areas for the CH₃(ads) on step and terrace sites, obtained by fitting the sum of two Gaussians to the measured RAIRS signal as a function of incident dose. We observed a much faster CH₃(ads) uptake on the steps than on the terraces, indicating a higher reactivity on the lower coordinated step sites. This is consistent with calculated barrier heights for the dissociation of CH₄ on steps and terraces of Pt(211) and in agreement with our assignment of the RAIRS signals for CH₃(ads) on step and terrace sites.

In order to test if CH₃(ads) diffusion occurs at $T_s = 120$ K on Pt(211) as proposed by Papp et al. [31] for Pt(533) and Pt(322) [31], Pt(211) was exposed to a beam of CH₄ with $E_{\text{trans}} = 56$ kJ/mol. Figure 6 shows that at low incident energy, CH₃(ads) uptake occurs selectively on the steps, confirming the lower barrier for methane dissociation on the steps compared to the terraces. After 15 min deposition at $E_{\text{trans}} = 56$ kJ/mol and with the steps now saturated with CH₃(ads), the molecular beam deposition was stopped

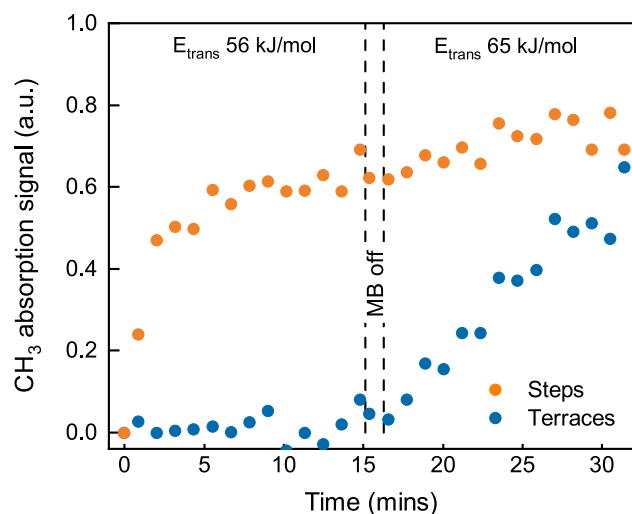


Fig. 6 RAIRS uptake curves for methane dissociation on the terraces (blue) and steps (orange) of Pt(211) for $T_s = 120$ K [80]. During the first 15 min, the incident translational energy of CH_4 was $E_{\text{trans}} = 56$ kJ/mol and $\text{CH}_3(\text{ads})$ is detected only on the steps. For $t > 16$ min, E_{trans} was raised to 65 kJ/mol, leading to $\text{CH}_3(\text{ads})$ uptake also on the terrace sites

for 2 min. If dissociation also occurred on the terraces at $E_{\text{trans}} = 56$ kJ/mol and rapid diffusion caused the $\text{CH}_3(\text{ads})$ to move to the step sites as proposed by Papp et al., we would expect to detect an increase in the terrace peak height at $E_{\text{trans}} = 56$ kJ/mol once the steps are saturated. This is not observed in Fig. 6. The terrace peak only starts to grow when the incident energy is raised to $E_{\text{trans}} = 65$ kJ/mol. Therefore, we can exclude surface diffusion of $\text{CH}_3(\text{ads})$ at $T_s = 120$ K which is consistent with a calculated barrier of 64 kJ/mol [32] by DFT for methyl diffusion from the terraces to the steps.

3.1.2 Surface-Site-Specific Methane Sticking Coefficients

The slope of the RAIRS detected uptake curve shown in Fig. 5b is proportional to the coverage dependent sticking coefficient $S(\theta)$. In order to determine $S(\theta)$ from the uptake, we calibrated the RAIRS absorption signal in terms of adsorbate coverage on each specific surface site.

Using site-specific RAIRS detection, we can decompose the total sticking coefficient, measured for example by a K&W experiment into the contributions from the different surface sites present on the surface. For example for Pt(211) we can write:

$$S_0(\text{total}) = \rho_s \cdot S_0(\text{step}) + \rho_t \cdot S_0(\text{terrace}) + \rho_c \cdot S_0(\text{corner}) \quad (4)$$

where $S_0(\text{step})$, $S_0(\text{terrace})$, and $S_0(\text{corner})$ are the surface-site-specific sticking coefficients for step, terrace and corner sites each multiplied by the relative density ρ_i of the specific

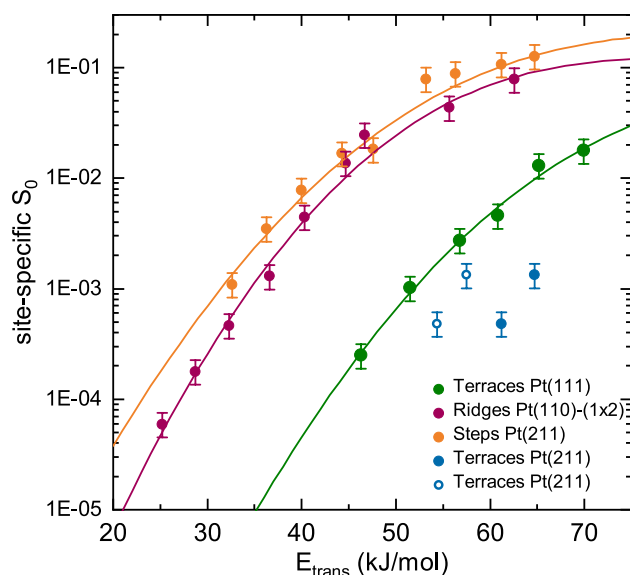


Fig. 7 Site-specific initial sticking coefficient S_0 vs. incident translational energy (E_{trans}): terrace sites of Pt(111) ($T_s = 150$ K, green) [80], the ridges of the Pt(110)-(1×2) surface ($T_s = 120$ K, red), and the steps (orange) and terraces (blue) of the Pt(211) surface ($T_s = 120$ K). The solid symbols are S_0 as a function E_{trans} measured normal to the macroscopic surfaces. The open symbol S_0 vs. E_{trans} normal to the (111) terrace of the Pt(211) surface which are tilted by 19.5° relative to the 211 crystal plane. The solid lines corresponds to the fit to the experimental data points obtained using Eq. (5)

surface site i . The contribution of the different sites to the total sticking coefficient S_0 depends on the incident translational energy E_{trans} due to the site-dependent dissociation barriers. For example, at low E_t , the total sticking coefficient S_0 is given exclusively by the contribution of the steps $\rho_s \cdot S_0(\text{step})$, since these are the sites with the lowest dissociation barrier, while with increasing E_{trans} the contribution of the terrace sites increases.

The definition of site-specific initial sticking coefficients allows for comparison of the specific reactivity on different surface sites. In order to determine the surface-site-specific sticking coefficients from the site-specific RAIRS uptake curves, we need to know the incident dose on each of the different surface sites. To do so, the total incident dose on the surface calculated from Eq. (1) is converted to the fractional dose on each site. On the Pt(211) surface, the fractional dose on each site (step, terrace and corner) is assumed to be 1/3 of the total incident dose since the surface layer consists of these three types of atoms in equal proportion. On the Pt(110)-(1×2) surface, the incident dose on the ridge atoms is assumed to be 1/4 of the total incident dose.

Figure 7 shows a comparison of the site-specific S_0 values for the different sites on three different Pt surfaces as a function of incident translational energy. To better visualize the

trend in S_0 as a function of incident energy, we fitted so-called S-shaped reactivity curves [2] to the data points:

$$S_0 = \frac{A}{2} \left[1 + \operatorname{erf} \left(\frac{E_{\text{trans}} - E_0}{W} \right) \right] \quad (5)$$

where A is the asymptotic value of S_0 at high incident energy, E_0 is the average activation barrier height and W is the width of the distribution of barrier heights assumed to be Gaussian.

For all the incident energies studied, we observed the highest reactivity for the lowest coordinated step and ridge sites. This is consistent with the reactivity ordering predicted by the DFT-PBE results described below. The DFT-PBE activation energy barrier we have obtained for dissociation on the Pt(211)-T sites is higher than on Pt(211)-S sites, in agreement with results reported in a previous study [32]. Still, the present difference between both activation energies is smaller than the one of Ref. [32]: 38 kJ/mol vs. 55 kJ/mol.

We find the Pt(110)-(1×2) ridge sites to have a slightly lower sticking coefficient than the step sites on Pt(211) while both have the same coordination number $CN=7$. This is in qualitative agreement with the theoretical results presented here and previously reported [32, 39]. By fitting the measured kinetic energy dependence of the site-specific sticking coefficients S_0 both for the steps and the ridges using Eq. (5) with a constant asymptote A and width W for the distribution of barrier heights, we obtain an average activation barrier height $E_0 \sim 3$ kJ/mol higher for the ridges than for the steps. This difference in the average barrier height obtained experimentally is smaller than the difference in the minimum barriers for dissociation on the steps and ridges calculated using DFT. Our PBE results predict a minimum energy barrier on ridge sites higher than on the steps by 29 kJ/mol. This value is slightly larger than the one reported by B. Jackson and co-workers (also using the PBE functional but without accounting for surface relaxation during the calculation of the transition state geometry): 22 kJ/mol higher on the ridges than on the steps [32, 39]. Interestingly, using a specific reaction parameter (SRP) XC functional, Chadwick et al. [70] predicted a barrier on the ridges higher than on the steps by only 10 kJ/mol which is closer to the experimental value observed here.

Recently, we reported a comparison between the experimental sticking coefficients for Pt(110)-(1×2) measured at $T_S = 650$ K using the K&W method and the ones predicted by ab initio quasi-classical trajectory calculations using the latter SRP XC functional [70]. Both agree very well at high incident energies but disagree for incident energies lower than 110 kJ/mol. Good agreement was found between the calculated and measured reactivities at low energies as long

as some contribution to the dissociation from molecules trapped on the surface was included.

This trapping mediated channel on Pt(110)-(1×2) could explain why the measured reactivities are larger than predicted by theory without including this trapping channel. However, the existence of trapping mediated dissociation could not be confirmed by our experiments. The lifetime of physisorbed CH_4 on Pt(110)-(1×2) at $T_S = 120$ K is around 32 ms [70]. Taking into account the flux of incident molecules on the surface, we expect to have less than 1% of a ML of CH_4 on the surface, which is below our limits of detection.

Another interesting feature shown in Fig. 7 is a difference in the sticking coefficient between the terraces of the flat Pt(111) surface and the terraces of Pt(211) which were assumed to be identical in previous studies [28, 31]. Although both sites have the same coordination number ($CN=9$), the Pt(111) terrace sites are more reactive. A possible reason for this discrepancy is the different normal incident energies onto the terraces of Pt(111) and Pt(211) surface. Since the (111) microfacets of the Pt(211) surface are tilted with respect to the macroscopic (211) surface plane by 19.5° , the incident normal energy onto the 211 terraces is lower by a factor of $\cos [2] (19.5^\circ) = 0.63$ compared to the 111 terraces for a molecular beam incident normal the macroscopic surface plane. Using this correction for the local normal incident energy, we obtained the open symbols shown in Fig. 7, which are in better agreement with the S_0 on the terraces of Pt(111). The remaining horizontal offset between the data points for Pt(111) and the corrected S_0 values for the terraces of Pt(211) is approximately 5 kJ/mol, close to the calculated difference between the DFT-PBE energy barriers for Pt(211)-T and Pt(111)-T sites of only 3 kJ/mol.

These results demonstrate that the coordination number of the surface atoms where absorption takes place is not the only factor which determines the site-specific reactivity and that the local environment surrounding the surface site also plays a role. Calle-Vallejo et al. [71] proposed the use of the generalized coordination number (CN) that takes into account the coordination number of the nearest neighbor atoms. Therefore, this number can take into account the main difference between the (111) terrace of the stepped and the flat surfaces as well as the difference between the steps on Pt(211) and the ridges of Pt(110)-(1×2). However, the generalized coordination number is higher on the terraces of the Pt(111) surface ($CN=7.5$) than on the terraces of the Pt(211) ($CN=7.33$), and it is also higher on the steps of Pt(211) ($CN=5.5$) than on the ridges of the Pt(110)-(1×2) ($CN=5.16$). Therefore, a higher reactivity would be expected on the terrace sites of the Pt(211) than on the terrace sites of Pt(111), and

Table 2 DFT-PBE results for the minimum dissociation barrier height for CH₄ chemisorption, E_b, adsorption energy of CH₃, E_{ads}[CH₃], frequency of the symmetric stretching mode of CH₃, and

some relevant interatomic distances in the optimum chemisorption geometry for the methyl group

Surface-site	E _b (kJ/mol)	E _{ads} [CH ₃] (kJ/mol)	ν _{sym} (cm ⁻¹)	<d _{C-H} > (Å)	d _{C-Pt1} (Å)	d _{H-Pt1} (Å)	d _{H-Pt2} (Å)
Pt(111)-T	64	-198	2973	1.097	2.067	2.625–2.626–2.625	3.211–3.225–3.241
Pt(211)-T	67	-207	2977	1.097	2.060	2.608–2.614–2.623	3.213–3.205–3.223
Pt(211)-S	30	-218	2969	1.098	2.056	2.595–2.627–2.630	3.152–3.423–3.665
Pt(110)-F	–	-195	2962	1.098	2.065	2.639–2.615–2.609	3.364–3.220–3.362
Pt(110)-R	59	-193	2964	1.098	2.054	2.628–2.605–2.610	3.666–3.406–3.144

a higher reactivity would be expected on the ridges of Pt(110)-(1 × 2) than on the steps of Pt(211) opposite to the experimental results observed here. We suggest that the slightly higher reactivity of Pt(111)-T sites compared with Pt(211)-T ones, might be due to the 2% compression of T Pt atoms of Pt(211), provoked by the relaxation of the stepped surface (see below).

3.2 Theory

Energetic and geometrical aspects of CH₄, CH₃, and H adsorption on Pt(111), Pt(211), and Pt(110)-(1 × 2), including the energy of transition states for CH₄ dissociation, have been studied previously by DFT calculations by a number of authors [21, 32, 35–42, 72, 73]. However, the use of different theoretical models complicates a direct comparison of the results for various systems among each other, and with our experiments. Moreover, vibrational frequencies of the chemisorbed methyl groups and their surface site dependence have not been predicted by theory to the best of our knowledge. Therefore, here we report results of new DFT calculations. With the DFT settings mentioned above in Section III.b., the minimum dissociation barriers for CH₄ dissociation on Pt(111)-T, Pt(211)-T, Pt(211)-S, and Pt(110)-(1 × 2)-R are: 64 kJ/mol, 67 kJ/mol, 30 kJ/mol, and 59 kJ/mol respectively (see Table 2). We have considered only T and S sites for Pt(211) and R ones for Pt(110)-(1 × 2) because previous theoretical studies [32, 74] have estimated the corresponding activation energy barriers on other sites, to be too high to be accessible in the experimental conditions considered in this work. The E_b values reported here slightly differ from those reported previously in the literature due to several reasons that include the use of a rigid surface model by other authors, different XC functionals, number of Pt layers to model the surface, size of the supercells, k-point meshes, and energy cut-offs [21, 32, 37, 39, 40, 57]. Still, as far as the relative reactivity is concerned (taking the E_b as the prescriptor), our results agree well with them, and predict the following ordering for reactivity: Pt(211)-S > Pt(110)-(1 × 2)-R > Pt(111)-T > Pt(211)-T. Interestingly, the CH₄ activation energy on Pt(211)-S sites is significantly

smaller than on the other three sites for which the dissociation barriers are close to each other. Since the coordination numbers of S Pt atoms of Pt(211) and Pt(110)-(1 × 2) are both CN = 7 and the dissociation barrier height in the former case is calculated to be 29 kJ/mol smaller than in the latter, it is clear that other ingredients (not only the coordination number) do play an important role for reactivity, in line with our experiments (see above). In addition, both Pt(111)-T and Pt(211)-T have CN = 9 and the barrier on the latter Pt atom is calculated to be larger than on the former by 3 kJ/mol. This relatively small difference between barriers on the two T sites is likely due to a compressive strain effect. The average distance between the Pt(211)-T atoms and their nearest neighbor (NN) exposed Pt's is 2% smaller than the NN distance between Pt atoms in the flat Pt(111) surface due to the stepped (211) surface relaxation. Such a compressive strain produces a downshift of the d-band center for metal atoms with more than half-filling of the d-band like Pt which in turn (according to the d-band model [75–77]) provokes a decrease of reactivity.

In Table 2, we report minimum dissociation barrier heights for CH₄, adsorption energies for CH₃, interatomic distances relevant for the optimum adsorption geometries, and the vibrational frequency of the symmetric C–H stretch mode ν_{sym} for CH₃ chemisorbed on Pt(111), Pt(211), and Pt(110)-(1 × 2). On Pt(211)-S, |E_{ads}[CH₃]| is larger than on Pt(211)-T by ~ 10 kJ/mol consistent with the higher reactivity for lower coordinated step atoms. It is interesting to note that the reactivity ordering deduced from the barrier heights is not respected if we take the adsorption energy of CH₃ as a probe of reactivity. In fact, on Pt(110)-(1 × 2)-S, |E_{ads}[CH₃]| is the smallest (weakest CH₃-surface bond), whereas the activation energy for CH₄ dissociation on this site is the second smallest one among all the sites we have investigated. Still, all the values of E_{ads}[CH₃] shown in Table 2 are close to each other, differences being ≤ 10%.

For CH₃ chemisorbed on T sites of Pt(111) and Pt(211), the ν_{sym} values are close to each other: 2973 cm⁻¹ and 2977 cm⁻¹. This further validates the assignment of the RAIRS peak of CH₃ on T sites of Pt(211) described above. On the other hand, the frequencies computed for CH₃

Table 3 Influence of the choice of the electronic exchange–correlation functional and van der Waals interaction on the CH₄ physisorption energy, CH₃ adsorption energy, and frequency of the symmetric stretching mode of the chemisorbed CH₃ on Pt(211)

	Pt(111) ($2 \times \sqrt{3}$) supercell		Pt(211)	
	Terrace (T)		Terrace (T)	Step (S)
$E_{\text{ads}}[\text{CH}_4]$ (kJ/mol)				
PBE	–3		–2	–3
PBE-D3	–27		–30	–23
optPBE-vdW	–25		–22	–18
$E_{\text{ads}}[\text{CH}_3]$ (kJ/mol) and $d_{\text{C-Pt}}$ (Å)				
PBE	–198 and 2.067		–207 and 2.060	–218 and 2.056
PBE-D3	–230 and 2.067		–243 and 2.057	–243 and 2.054
optPBE-vdW	–226 and 2.074		–236 and 2.067	–238 and 2.062
ν_{sym} (cm ^{–1})				
PBE	2973		2977	2969
PBE-D3	2967		2969	2961
optPBE-vdW	2945		2949	2940

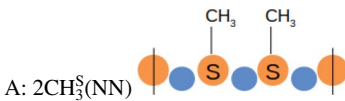

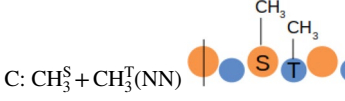
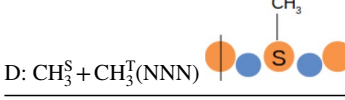
chemisorbed on S sites are also close to each other: 2969 cm^{–1} and 2964 cm^{–1} but smaller than the frequencies corresponding to T sites, the latter finding being in contrast with experiments. Interestingly, the frequencies predicted for CH₃/Pt(110)-(1 × 2)-V and CH₃/Pt(110)-(1 × 2)-R are rather close (2962 cm^{–1} vs. 2964 cm^{–1}) which might entail a difficulty for the use of RAIRS to perform site-selective reactivity measurements even in conditions under which dissociation on both T and S Pt atoms of Pt(110)-(1 × 2) could be possible. However, the frequency difference between CH₃/Pt(211)-S and CH₃/Pt(211)-T measured by RAIRS is $\Delta\nu = \nu_{\text{sym}}^{\text{S}} - \nu_{\text{sym}}^{\text{T}} = +17$ cm^{–1}, while our DFT-PBE results predict a shift in the opposite direction with $\Delta\nu = -8$ cm^{–1}.

In order to elucidate the origin of this discrepancy, we compare the adsorption geometries of CH₃ on S and T Pt atoms in Table 2, where we report the values of the C–Pt and C–H bond lengths ($d_{\text{C-Pt}}$, and $d_{\text{C-H}}$), as well the distance between each H atom of the methyl group and its nearest Pt neighbor (NN), and next nearest Pt neighbor (NNN): $d_{\text{H-Pt1}}$ and $d_{\text{H-Pt2}}$ respectively. In all cases, the Pt atom that is NN to the H atoms is the binding site of the CH₃ group. We find similar values for $d_{\text{C-Pt}}$, $d_{\text{C-H}}$, and $d_{\text{H-Pt1}}$ for all adsorption geometries. However, there are differences between the values of $d_{\text{H-Pt2}}$, for CH₃ adsorption on a T or S Pt atom. In particular, whereas on a T Pt atom, the three values of $d_{\text{H-Pt2}}$ are all ~3.2 Å, on a S Pt atom the three values of $d_{\text{H-Pt2}}$ are ~3.2 Å, 3.4 Å, and 3.6 Å. Therefore, when CH₃ is adsorbed on a T Pt atom the C–H bonds are closer and can interact slightly stronger with the Pt surface (see Fig. 2). This might cause a stronger softening of the C–H bonds and consequently, a frequency of CH₃ bound to a T Pt atom, might become smaller than for CH₃ on a S Pt atom as observed experimentally [32]. In fact, this is the effect that produces for CH₃ adsorbed on a fcc-hollow site of Pt(111), a frequency ~200 cm^{–1} smaller

than on top, despite the smaller binding energy of CH₃ in the former site [36]. However, our DFT-PBE results for the vibrational frequencies do not confirm this hypothesis which could be due to the large $d_{\text{H-Pt2}}$ values and the well-known failure of the PBE functional to describe of long-range dispersion forces.

In order to investigate the possible effect of long-range van der Waals interactions on the vibrational frequencies of CH₃ on S and T Pt atoms, we have also performed calculations using the PBE-D3 method [57], and with the optPBE-vdW XC functional [56]. As indicated in Table 3, these calculations for Pt(111) have been performed for a $2 \times \sqrt{3}$ supercell. We previously verified that the choice of functional affects neither the adsorption energies nor the vibrational frequencies. As expected, the adsorption energies for the physisorption of CH₄ (due to van der Waals interactions) obtained with PBE-D3 and optPBE-vdW are significantly larger than for PBE since the latter largely underestimates the depth of physisorption wells. PBE-D3 predicts physisorption energies larger than optPBE-vdW, both being in reasonable agreement with the estimated desorption energy extracted from temperature programmed desorption (TPD) results [78]. Interestingly, both calculations that incorporate vdW interactions predict a much smaller difference in adsorption energy for CH₃ on S and T sites of Pt(211) than PBE. This is consistent with the long-range dispersion forces contributing to the interaction of C–H bonds with Pt atoms for CH₃ in T sites more than for S sites. However, the frequencies reported in Table 3 show that this does not entail a significant change in the value of $\Delta\nu = \nu_{\text{sym}}^{\text{S}} - \nu_{\text{sym}}^{\text{T}}$ obtained with PBE. The predicted value by DFT for ν_{sym} for CH₃ chemisorbed on S sites is, for all the methods we have used, ~8–9 cm^{–1} smaller than on T sites which is at odds with experiment.

Table 4 Lateral interaction between methyl groups chemisorbed on Pt(211)

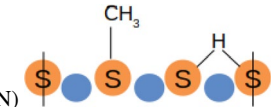
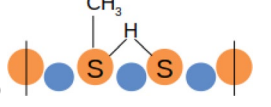
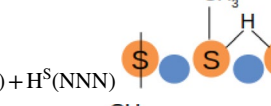
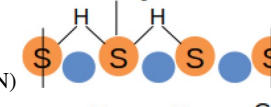
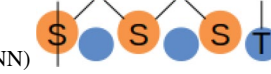
$2\text{CH}_3/\text{Pt}(211)$ conf.	$E_{\text{ads}}[\text{CH}_3]$ (kJ/mol)	ν_{sym} (cm^{-1})
 A: $2\text{CH}_3^{\text{S}}(\text{NN})$	-214	2968(S)–2966(S)
 B: $2\text{CH}_3^{\text{T}}(\text{NN})$	-203	2978(T)–2976(T)
 C: $\text{CH}_3^{\text{S}} + \text{CH}_3^{\text{T}}(\text{NN})$	-211	2975(T)–2966(S)
 D: $\text{CH}_3^{\text{S}} + \text{CH}_3^{\text{T}}(\text{NNN})$	-213	2972(T)–2963(S)

In the schematic representation of the configurations considered (side view of the 1×3 cell), T and S Pt atoms are represented in orange and blue respectively. For simplicity C Pt atoms are not included in the scheme

In view of this discrepancy with experiments, we have also investigated the effect of co-adsorbed species. Since RAIRS experiments are performed at a low surface temperature (120–150 K), well below the values for desorption of hydrogen atoms (forming H_2) and full decomposition of CH_3 , it is useful to investigate how the presence of co-adsorbed $\text{CH}_3(\text{ads})$ and $\text{H}(\text{ads})$ affects the vibrational frequency of $\text{CH}_3(\text{ads})$. In Table 4, we show the average adsorption energy per methyl group, $E_{\text{ads}}[\text{CH}_3]$, when two CH_3 groups are adsorbed simultaneously within the 1×3 supercell, making the coverage twice the value considered above. We have considered four different situations: (A) two CH_3 adsorbed on S Pt atoms NN with respect to each other, (B) two CH_3 adsorbed on T Pt atoms NN with respect to each other, (C) two CH_3 , one on a S Pt atom and the other on a T Pt atom, and NN with respect to each other, and (D) two CH_3 , one on a S Pt atom and the other on a T Pt atom, and NNN with respect to each other. The average adsorption energies show that the lateral interactions are rather weak, e.g. between ~ 4 and 5 kJ/mol per molecule for two CH_3 adsorbed on equivalent (T or S) Pt atoms that are NN to each other, and ~ 0 – 2 kJ/mol for two CH_3 adsorbed on non-equivalent NN Pt atoms. This weak lateral interaction could in principle allow two or more methyl groups to stay adsorbed close to each other entailing some change of the position and shape of the RAIRS peaks for high enough doses of methane on the surface. However, for all the structures considered, the frequency of CH_3 on a T (S) Pt atom remains between 2963 and 2968 cm^{-1} (2972 and 2978 cm^{-1}). Thus, the CH_3 frequency is only slightly affected by the presence of other methyl groups adsorbed nearby. Thus, our DFT results are in line with the relatively minor effect of co-adsorbed methyl groups on the RAIRS frequencies of $\text{CH}_3(\text{ads})$ on T and S sites for Pt(211).

In order to also consider the effect of co-adsorbed H atoms, we have computed the adsorption energy of CH_3 and its vibrational frequency, in presence of one and two co-adsorbed H atoms in five different configurations (see Table 5). This requires the search of possible adsorption sites for a single H atom on Pt(211). We have found that H atoms prefer adsorption in a bridge configuration between two NN S Pt atoms, and the corresponding value of $E_{\text{ads}}[\text{H}]$ is -278 kJ/mol. This optimum adsorption geometry and its E_{ads} value are both in good agreement with the results of previous DFT investigations for H/Pt(211) [73]. From the results of Table 5, it is clear that the presence of co-adsorbed H atoms affects the adsorption of CH_3 more strongly than the presence of other CH_3 groups (compare with Table 4). This is the case in particular for configurations in which both the CH_3 group and a H co-adsorbed atom are bound to the same surface Pt atom. Comparing the E_{ads} values of configurations E and F with the -218 kJ/mol value obtained without H atoms co-adsorbed (see Table 2) we can see that shearing a Pt atom between CH_3 and H (as in configuration F) has an energy cost of 19 kJ/mol. In contrast, the presence of one H atom bound to Pt atoms that are NN of the Pt one where CH_3 is bound (configuration E), slightly stabilizes chemisorption of CH_3 by 4 kJ/mol likely due to the lattice relaxation induced by the presence of H. In any case, the presence of only one co-adsorbed H atom does not affect the frequency of CH_3 , the frequencies obtained for configurations E and F being both the same (2967 cm^{-1}) and very close to the one obtained without H, i.e. 2969 cm^{-1} (Pt(211)-S in Table 2). The E_{ads} values obtained with two co-adsorbed H atoms (configurations G and H in Table 5) follow the same tendency. Adding an extra H atom “far” from CH_3 to configuration F (see configuration G) provokes a slight stabilization of CH_3 chemisorption whereas adding other H atom near CH_3

Table 5 $E_{\text{ads}}[\text{CH}_3]$ with co-adsorbed H atoms on Pt(211)

$[\text{CH}_3 + \text{mH}]/\text{Pt}(211)$ conf.	$E_{\text{ads}}[\text{CH}_3]$ (kJ/mol)	ν_{sym} (cm^{-1})
E: $\text{CH}_3^{\text{S}} + \text{H}^{\text{S}}(\text{NNN})$ 	-222	2967
F: $\text{CH}_3^{\text{S}} + \text{H}^{\text{S}}(\text{NN})$ 	-200	2967
G: $\text{CH}_3^{\text{S}} + \text{H}^{\text{S}}(\text{NN}) + \text{H}^{\text{S}}(\text{NNN})$ 	-203	2976
H: $\text{CH}_3^{\text{S}} + 2\text{H}^{\text{S}}(\text{NN})$ 	-176	2992
I: $\text{CH}_3^{\text{T}} + 2\text{H}^{\text{S}}(\text{NNN})$ 	-210	2978

In the schematic representation of the configurations considered (side view of 1×3 cell), T and S Pt atoms are represented in orange and blue respectively. For simplicity C Pt atoms are not included in the scheme

(configuration H) entails an extra energy cost of $-176 \text{ kJ/mol} - (200 \text{ kJ/mol}) = 24 \text{ kJ/mol}$. This clearly shows that H atoms prefer to occupy bridge sites [in the step of Pt(211)] without sharing any Pt atom with CH_3 . Interestingly, the presence of an increasing number of H atoms decorating the step near CH_3 , provokes an increase of the frequency of CH_3 chemisorbed on Pt(211)-S. However, due to the previous energetic considerations, it is not likely that frequency of CH_3 on Pt(211)-S larger than for Pt(211)-T obtained experimentally, could be due to the presence of co-adsorbed H atoms since at low surface coverages, H atoms will be able to diffuse along the step to stay far away from CH_3 (in configurations with significantly lower energies) where the effect on the CH_3 frequency is negligible. This is also in line with the negligible effect of coverage on the CH_3 frequencies observed experimentally. Finally, it is interesting to note in Table 5, that among the three configurations we have considered with two co-adsorbed H atoms (G, H, and I), the most stable one is that with the two H atoms chemisorbed in the step and CH_3 chemisorbed on a T Pt atom: i.e. configuration I. This means that in the competition for step sites, H atoms win over CH_3 and so, at relatively large coverages when there is not enough free S Pt atoms, the H atoms are the ones that will occupy step sites pushing the CH_3 groups to stay chemisorbed in T sites. However, the coverages for which such methyl displacement by H atoms is likely to take place is much larger than the highest coverage attained in our RAIRS experiments. To summarize the results of our analysis of coverage effects, we have found that for the low and moderate coverages involved in the

RAIRS experiments, the presence of neither CH_3 nor H atoms are likely to significantly affect the frequencies of CH_3 chemisorbed on Pt(211)-S and Pt(211)-T sites in line with experiments.

4 Summary and Conclusions

We report a combined experimental/theoretical investigation of methane dissociation on terrace (T), step (S), and ridge (R) sites of the Pt(111), Pt(211), and Pt(110)-(1×2) surfaces. Reflection Absorption Infrared absorption spectroscopy (RAIRS) is used for the surface site specific detection of chemisorbed methyl species on terrace, step and ridge atoms and to measure surface site specific methyl uptake curves. The uptake curves are used to calculate site specific sticking coefficients of CH_4 on the different surface sites of these three surfaces. For each surface, we observe evidence for a direct chemisorption mechanism and the absence of $\text{CH}_3(\text{ads})$ diffusion from the terraces to the step sites on Pt(211) at $T_s < 150 \text{ K}$. The experimental sticking coefficients for different surface sites are in agreement with calculated dissociation barrier heights for methane dissociation by density functional theory (DFT) which predicts the lowest dissociation barrier for the step sites on Pt(211), followed by the ridge sites on Pt(110)-(1×2), the terrace sites of Pt(111) and finally the terrace sites on Pt(211). DFT results confirm that the weak or absent dependence of the frequency and shape of the RAIRS peaks of $\text{CH}_3(\text{ads})$ are due to a weak interaction between methyl groups even when chemisorbed

on top of neighbouring Pt atoms. In addition, the moderate coverages produced experimentally prevent the frequency upshift that might result from (energetically unfavored) moieties involving two H atoms and a methyl group bound all to the same Pt atom. Our DFT results predict RAIRS frequencies for CH₃(ads) on step and terrace sites opposite to what is observed experimentally on Pt(211). This discrepancy indicates that either DFT is not able to predict the correct RAIRS frequencies, or that the species adsorbed on the steps and terraces product of the dissociation are different. Further investigation is needed to resolve this disagreement between experiment and theory.

Acknowledgements This work was supported by the Consejo Nacional de Investigaciones Científicas Técnicas (CONICET) and Ministerio de Educación, Cultura, Ciencia y Tecnología (ME) of Argentina and the Swiss National Science Foundation under the Argentinian-Swiss Joint Research Program (ASJRP) Project Nr. IZSAZ2-173328 as well as the ANPCyT Project PICT No. 2750 (ME-Argentina), and the UNR project PID ING534. M.E.T and H.F.B acknowledge computer time provided by CCT-Rosario Computational Center, and Centro de Simulación Computacional para Aplicaciones Tecnológicas (CSC), members of the High Performance Computing National System (SNCAD, ME-Argentina).

References

- Chorkendorff I, Niemantsverdriet JW (2003) Concepts of modern catalysis and kinetics. Wiley-VCH, Weinheim
- Juurlink LBF, Killelea DR, Utz AL (2009) Prog Surf Sci 84:69
- Utz AL (2009) Curr Opin Solid State Mater Sci 13:4
- Chadwick H, Beck RD (2017) Annu Rev Phys Chem 68:39
- Chadwick H, Beck RD (2016) Chem Soc Rev 45:3576
- Rettner CT, Pfnür HE, Auerbach DJ (1985) Phys Rev Lett 54:2716
- Rettner CT, Pfnür HE, Auerbach DJ (1986) J Chem Phys 84:4163
- Juurlink L, McCabe P, Smith R, DiCologero C, Utz AL (1999) Phys Rev Lett 83:868
- Hundt PM, Jiang B, van Reijzen ME, Guo H, Beck RD (2014) Science 344:504
- Bisson R, Dang TT, Sacchi M, Beck RD (2008) J Chem Phys 129:081103
- Beck RD, Maroni P, Papageorgopoulos DC, Dang TT, Schmid MP, Rizzo TR (2003) Science 302:98
- Smith RR, Killelea DR, DelSesto DF, Utz AL (2004) Science 304:992
- Bisson R, Sacchi M, Dang TT, Yoder B, Maroni P, Beck RD (2007) J Phys Chem 111:12679
- Bisson R, Sacchi M, Beck RD (2010) Phys Rev B 82:121404
- Donald SB, Harrison I (2012) Phys Chem Chem Phys 14:1784
- DeWitt KM, Valadez L, Abbott HL, Kolasinski KW, Harrison I (2006) J Phys Chem B 110:6705
- Abbott HL, Bukoski A, Harrison I (2004) J Chem Phys 121:3792
- Lozano A, Shen XJ, Moiraghi R, Dong W, Busnengo HF (2015) Surf Sci 640:25
- Guo H, Jackson B (2015) J Phys Chem C 119:14769
- Jiang B, Guo H (2013) J Phys Chem C 117:16127
- Migliorini D, Chadwick H, Nattino F, Gutiérrez-González A, Dombrowski E, High EA, Guo H, Utz AL, Jackson B, Beck RD, Kroes GJ (2017) J Phys Chem Lett 8:4177
- Nattino F, Migliorini D, Bonfanti M, Kroes GJ (2016) J Chem Phys 144:044702
- Kroes GJ (2015) J Phys Chem Lett 6:4106
- Sabbe MK, Reyniers MF, Reuter K (2012) Catal. Sci Technol 2:2010
- Vattuone L, Savio L, Rocca M (2008) Surf Sci Rep 63:101
- Libuda J, Freund HJ (2005) Surf Sci Rep 57:157
- Juurlink L (2018) J Phys: Condens Matter 30:090301
- Gee AT, Hayden BE, Mormiche C, Kleyn AW, Riedmüller B (2003) J Chem Phys 118:3334
- King DA, Wells MG (1972) Surf Sci 29:454
- Badan C, Koper MTM, Juurlink LBF (2015) J Phys Chem C 119:13551
- Papp C, Tränkenschuh B, Streber R, Fuhrmann T, Denecke R, Steinrück HP (2007) J Phys Chem C 111:2177
- Chadwick H, Guo H, Gutiérrez-González A, Menzel JP, Jackson B, Beck RD (2018) J Chem Phys 148:014701
- Jackson B, Nave S (2011) J Chem Phys 135:114701
- Nave S, Tiwari AK, Jackson B (2014) J Phys Chem A 118:9615
- Papioian G, Nørskov JK, Hoffmann R (2000) J Am Chem Soc 122:4129
- Michaelides A, Hu P (2001) J Chem Phys 114:2523
- Petersen MA, Jenkins SJ, King DA (2004) J Phys Chem B 108:5909
- Ford DC, Xu L, Mavrikakis M (2005) Surf Sci 587:159
- Nave S, Tiwari AK, Jackson B (2010) J Chem Phys 132:054705
- Chen Y, Vlachos DG (2010) J Phys Chem C 114:4973
- Viñes F, Lykhach Y, Staudt T, Lorenz MPA, Papp C, Steinrück HP, Libuda J, Neyman KM, Görling A (2010) Chem A Eur J 16:6530
- Qi Q, Wang X, Chen L, Li B (2013) Appl Surf Sci 284:784
- Mukerji RJ, Bolina AS, Brown WA (2003) Surf Sci 527:198
- Gutiérrez-González A, Crim FF, Beck RD (2018) J Chem Phys 149:074701
- Chen L, Ueta H, Bisson R, Beck RD (2013) Rev Sci Instrum 84:053902
- Scoles G (1988) Atomic and molecular beam methods. Oxford University Press, New York
- Speller S, Kuntze J, Rauch T, Bömermann J, Huck M, Aschoff M, Heiland W (1996) Surf Sci 366:251
- Tate MR, Gosálvez-Blanco D, Pullman DP, Tsekouras AA, Li YL, Yang JJ, Laughlin KB, Eckman SC, Bertino MF, Ceyer ST (1999) J Chem Phys 111:3679
- Blöchl PE (1994) Phys Rev B 50:17953
- Kresse G, Hafner J (1993) Phys Rev B 47:558
- Kresse G, Hafner J (1994) Phys Rev B 49:14251
- Kresse G, Furthmüller J (1996) Comput Mater Sci 6:15
- Kresse G, Furthmüller J (1996) Phys Rev B 54:11169
- Kresse G, Joubert D (1999) Phys Rev B 59:1758
- https://cms.mpi.univie.ac.at/wiki/index.php/The_VASP_Manual
- Perdew JP, Burke K, Ernzerhof M (1996) Phys Rev Lett 77:3865
- Grimme S, Antony J, Ehrlich S, Krieg H (2010) J Chem Phys 132:154104
- Klimeš J, Bowler DR, Michaelides A (2010) J Phys: Condens Matter 22:022201
- Chen L, Ueta H, Bisson R, Beck RD (2012) Faraday Discuss 157:285
- Oakes DJ, Mccoustra MRS, Chesters MA (1993) Faraday Discuss 96:325
- Bădescu C, Jacobi K, Wang Y, Bedürftig K, Ertl G, Salo P, Al-Nissila T, Ying SC (2003) Phys Rev B Condens Matter Mater Phys 68:205401
- Fairbrother DH, Peng XD, Trenary M, Stair PC (1995) J Chem Soc Faraday Trans 91:3619
- Deng R, Herceg E, Trenary M (2004) Surf Sci 573:310
- Jacob T, Goddard WA III (2005) J Phys Chem B 109:297
- Orita H, Inada Y (2005) J Phys Chem B 109:22469

66. Walsh AJ, van Lent R, Auras SV, Gleeson MA, Berg OT, Juurlink LBF (2017) *J Vac Sci Technol A Vac Surf Film* 35:03E102
67. Xu J, Yates JT (1995) *Surf Sci* 327:193
68. Bisson R, Sacchi M, Beck RD (2010) *J Chem Phys* 132:094702
69. Brandt RK, Sorbello RS, Greenler RG (1992) *Surf Sci* 271:605
70. Chadwick H, Gutiérrez-González A, Beck RD, Kroes GJ (2019) *J Chem Phys* 150:124702
71. Calle-Vallejo F, Tymoczko J, Colic V, Vu QH, Pohl MD, Morgenstern K, Loffreda D, Sautet P, Schuhmann W, Bandarenka AS (2015) *Science* 350:185
72. Petersen MA, Jenkins SJ, King DA (2004) *J Phys Chem B* 108:5920
73. Olsen RA, Bădescu ȘC, Ying SC, Baerends EJ (2004) *J Chem Phys* 120:11852
74. Anghel AT, Wales DJ, Jenkins SJ, King DA (2005) *Phys Rev B Condens Matter Mater Phys* 71:2
75. Hammer B, Nørskov JK (1995) *Surf Sci* 343:211
76. Hammer B, Nørskov JK (1995) *Nature* 376:238
77. Hammer B, Nørskov JK (2000) *Adv Catal* 45:71
78. Watanabe K, Matsumoto Y (1997) *Surf Sci* 390:250
79. Killelea DR, Campbell VL, Shuman NS, Smith RR, Utz AL (2009) *J Phys Chem C* 113:20618
80. Ueta H, Chen L, Beck RD, Colón-Díaz I, Jackson B (2013) *Phys Chem Chem Phys* 15:20526

Publisher's Note Springer Nature remains neutral with regard to jurisdictional claims in published maps and institutional affiliations.